GU J Sci 30(1): 139-159(2017)

Gazi University

Journal of Science

http://dergipark.gov.tr/gujs

Synthesis, Crystal Structure, Spectroscopic and Density Functional Modelling Studies of The 2-Isopropylbenzimidazolium Tetrachloroplatinate(II) Monohydrate

Celal Tuğrul ZEYREK[1,*], Hüseyin ÜNVER[2], Mahmut GOZELLE[3], Nefise DILEK[4], Fatma GÜMÜŞ[3]

[1]*Ankara Nuclear Research and Training Center, Turkish Atomic Energy Authority, 06100 Besevler-Ankara, Turkey.*

[2]*Department of Physics, Faculty of Sciences, University of Ankara, 06100 Besevler-Ankara, Turkey.*

[3]*Department of Pharmaceutical Chemistry, Faculty of Pharmacy, Gazi University, 06330 Etiler-Ankara, Turkey.*

[4]*Department of Physics, Faculty of Sciences and Arts, University of Aksaray, 68100 Aksaray, Turkey.*

Article Info

Received: 03/10/2016
Revised: 23/12/2016
Accepted: 23/12/2016

Keywords

Crystal structure
Platinate salts
Benzimidazole
Density functional
Theory
Hydrogen bond

Abstract

Synthesis, crystallographic characterization, spectroscopic and density functional modelling studies of the 2-isopropylbenzimidazolium tetrachloroplatinate monohydrate $(C_{10}H_{13}N_2)_2.[PtCl_4].H_2O$ have been reported. The molecular structure of the compound was determined by single-crystal X-ray diffraction analysis. In the compound, the Pt atoms reside at a center of inversion. The compound is comprised of 2-isopropylbenzimidazole $(Hipb)^+$: $(C_{10}H_{13}N_2)^+$ and $[PtCl_4]^{2-}$ ions, respectively, linked by intermolecular hydrogen bonds N···Cl [3.249(4) from 3.660(7) Å], C···Cl [range from 3.553(7) to 3.895(7) Å] and O atom of a non-coordinating water molecule in the crystal structure N···O [2.728(8) Å], O···Cl [range from 3.234(6) to 3.451(7) Å], C···O [range from 3.350(7) to 3.545(1) Å] for the investigated compound. The molecular structure obtained from X-ray single-crystal analysis of the investigated compound in the ground state has been compared using Hartree-Fock (HF) and density functional theory (DFT) with the functionals B3LYP and PBE1PBE using the LANL2DZ basis set. The experimental and calculated vibrational frequencies of the title compound have been compared. There exists a good correlation between experimental and theoretical data for the complex.

1. INTRODUCTION

The compounds having benzimidazole moieties have been used in the area of pharmaceuticals [1-5]. Various benzimidazole derivatives have been found to possess anticancer, antiviral, antihypertension and some other properties [4-7]. In analytical area, benzimidazole moieties have been investigated as reagents for the separation, concentration, and selective determination of many of the first row transition metal cations [8,9]. It is known that coordination with metals can modify the toxicological and pharmacological properties of benzimidazole moieties [10,11]. Cisplatin, [*cis*-$PtCl_2(NH_3)_2$] is a clinically important antitumor drug used in the treatment of testicular, ovarian, bladder, and head and neck cancers [12]. Nowadays, cisplatin, carboplatin and oxaliplatin are used treatment of various cancer types worldwide [13]. Most notably, long-term survival for rates of testicular cancer patients using cisplatin improved from less than 10% to greater than 90% [14].

Extensive evidence indicates that DNA is the critical target for the antitumor activity of cisplatin [15,16]. However, the drug's wide-spread use is limited by its major side effects which include nephrotoxicity, myelosuppression, ototoxicity, and other neurological disorders. Therefore, its clinical utility is restricted by both toxicological and especially tumor resistance considerations [17]. The need for cisplatin analogs which are less toxic and have a broader spectrum of activity led to the synthesis of a large number of platinum complexes over the past four decades. Replacement of the NH_3 groups by cyclic amines (especially those involving large rings) generally reduces the toxicity of the platinum compounds [18]. Several platinum complexes with N-heterocyclic ligands such as imidazol, thiazole, benzimidazole, benzoxazole, and benzothiazole have been reported [19-23].

*Corresponding author, e-mail: zeyrek@taek.gov.tr

In previous papers we reported the synthesis, characterization and in vitro cytotoxic activities of complexes of the structure *cis*-[Pt(L)$_1$ or $_2$ Cl2], where L is mono- or bidentate 2-substituted benzimidazole [21,24-28]. It was found that some of these new benzimidazole Pt(II) complexes have in vitro cytotoxic activities equal to cisplatin. Even though benzimidazole Pt(II) complexes have been studied extensively, there are only a few reports the on the platinum salts with benzimidazolium cations [29-31]. We reported the crystal structures of on the platinum salts 2-(3'-hydroxypropyl)benzimidazolium hexa- and tetrachloroplatinate [29]. In this study, we report the synthesis, crystallographic characterization, spectroscopic and computational [density functional theory (DFT)] modelling studies of the salt $[(Hipb)_2]^+.[PtCl_4]_2.H_2O$.

2. MATERIALS AND METHODS

2.1. Reagents and Techniques

All chemicals and solvents were obtained commercially (Merck and Sigma-Aldrich) and were used without further purification. The reactions were monitored by thin layer chromatography (TLC), which was performed on pre-coated aluminum plates (Silicagel F_{254}, Merck). Plates were visualized by UV light, Dragendorff reagent and iodine vapor. ^{1}H NMR spectra were recorded in DMSO-$_{d6}$ on a Varian Mercury 400 MHz High Performance Digital FT-NMR spectrometer using tetramethylsilane as the internal standard. All chemical shifts are reported in ppm (δ). Infrared absorption (IR) spectra were recorded on a Perkin Elmer Spectrum 400 FTIR/FTNIR spectrometer equipped with a Universal ATR Sampling Accessory and were reported in cm^{-1} units. Carbon, nitrogen and hydrogen analyses were performed on a LECO CHNS-932 elemental analyzer and were within ±0.4% of theoretical values. Melting points were determined with an SMP-II Digital Melting Point Apparatus and are uncorrected.

2.2. Synthesis of the Compound

2-Isopropylbenzimidazole was synthesized as reported by Chari et al. in 2011 (mp.237-238°C, lit mp.237-239°C) [32]. To a stirred solution of 2-isopropylbenzimidazole (268.6 mg, 1.68 mmol) in 0.5 N HCl (8 ml) was added drop wise a solution of K_2PtCl_4 (400.4 mg, 0.96 mmol) in 0.5 N HCl (10 ml) over 30 min at room temperature. The reaction mixture was protected from light and heated at 60 °C for 11 days. The resulting precipitate was filtered off and washed several times with water, ethanol, acetone and diethylether, afterwards dried in vacuum desiccator. This complex was characterized by its elemental analysis, IR and NMR. For obtain suitable crystals for X-ray diffraction, the compound dissolved in water by heating at 60 °C. The resulting solution was kept at 4 °C. After two days, red crystals suitable for X-ray diffraction were obtained. The crystals were characterized by X-ray diffraction. The chemical diagram of the $[(Hipb)_2]^+.[PtCl4]_2.H_2O$ is show in Fig. 1.

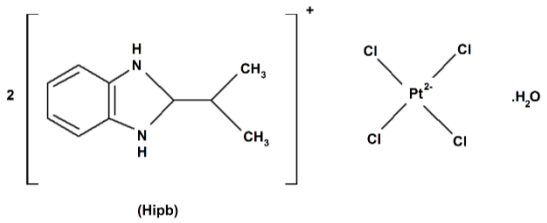

Figure 1. *Chemical diagram of 2-isopropylbenzimidazole tetrachloroplatinate monohydrate* $[(Hipb)_2]^+.[PtCl_4]_2.H_2O$.

Formula; $(C_{10}H_{13}N_2)_2.[PtCl_4]$, calcd. C 36.43, H 3.97, N 8.50; found C 36.19, H 4.18, N 8.57; Yield, 20.3 %. IR (ATR) (cm^{-1}); 3100, 3062, 2971, 2934, 2877, 2817, 2754, 2661, 1622, 1542, 1458, 1412, 1274, ^{1}H-NMR spectrum (DMSO-d_6) δ ppm; 7.808-7.784 (dd, J= 6,4 and 8 Hz, 4H, Aromatic H), 7,556-7,537 (dd, J= 6 and 8 Hz, 4H, Aromatic H), 3.529-3.459 (m, 2H, 2x Ar-CH-$(CH_3)_2$), 1.465 (d, J= 6,8 Hz, 12H, 2x CH-$(CH_3)_2$).

2.3. X-Ray Structure Determination

A crystal of dimension 1.50 x 0.45 x 0.35 mm^3 was mounted on a Bruker Smart Breeze CCD diffractometer Mo-K_α radiation (λ=0.71073 Å) [33]. The crystal data, intensity data collection details and refinement parameters are summarized in Table 1. The compound is solved by direct methods using SHELXS-97 [34] and refined with SHELXL-97 [35]. The refinement was carried out by full-matrix least-squares method on the positional and anisotropic temperature parameters of the non-hydrogen atoms. The scattering factors were taken from SHELXL-97 [35]. The positions of the H atoms bonded to carbon atoms were calculated [C–H distance 0.93Å], and included in the structure factor calculation using a riding model. The imidazole N atoms (HN) and H atoms of the water molecule were found from a difference Fourier map calculated at the end of the refinement process as a small positive electron density. The H atom displacement parameters were restricted to be 1.2 Ueq of the parent atom. ORTEP view of the molecular structure of the investigated compound is given in Fig. 2 and the crystal packing diagram is given in Fig. 3 [36]. Crystallographic data (excluding structure factors) for the structure reported in this paper have been deposited with the Cambridge Crystallographic Data Centre as Supplementary Publication No. CCDC 1044156[1].

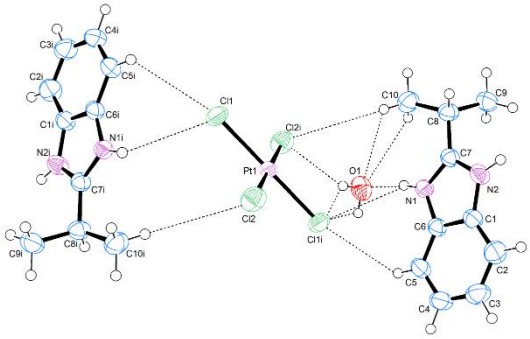

Figure 2. *Ortep-3 diagram of the title compound. Displacement ellipsoids are drawn at the 50% probability level. (Symmetry transformations used to generate equivalent atoms (i): −x, −y, −z).*

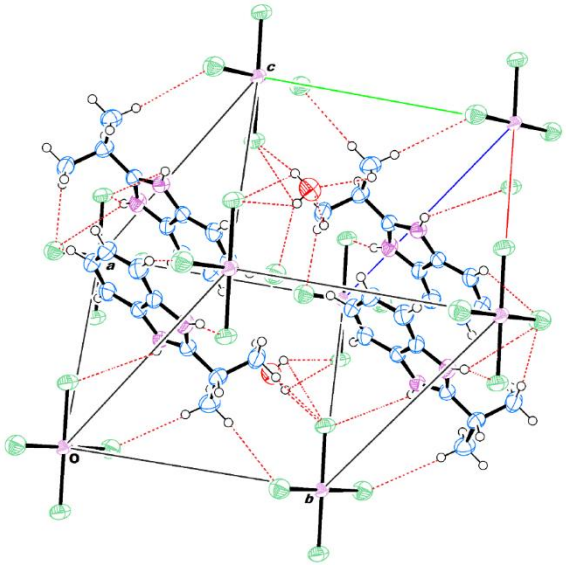

Figure 3. *Unit-cell packing diagram for the title compound. The intermolecular hydrogen bond is shown as a dashed line.*

Table 1. *Crystallographic data and structure refinement for the title compound.*

Sum formula	$(C_{10}H_{13}N_2)_2.[PtCl_4].H_2O$	
Crystal shape/color	Prism/Yellow	
Formula weight	445.24	
Crystal size (mm^3)	$0.40\times0.38\times0.23$	
Crystal system	Triclinic	
Space group	*P-1*	
Unit cell parameters	a = 8.1946(5) Å	α=63.854(2)
	b = 9.3595(5) Å	β=69.631(2)
	c = 9.8709(5) Å	γ=89.038(2)
Volume	628.66(6) $Å^3$	
Z	2	
D_x (Mg cm^{-3})	1.837	
μ (mm^{-1})	6.029	
Diffractometer/meas.meth	Bruker Smart Breeze CCD/w and φ-scans	
Absorption correction	Multi-scan	
Index ranges	$-10 \le h \le 10$	
	$-11 \le k \le -11$	
	$-12 \le l \le 12$	
No. of measured, independent and observed reflections	2565, 2562, 2565	
Criterion for observed reflections	$I > 2\sigma(I)$	
R_{int}	0.0293	
θ_{min} , θ_{max}	2.46, 26.37	
Refinement on	F^2	
R [$F^2 > 2\sigma(F^2)$], wR, S	0.0261, 0.0732, 1.081	
No. of reflection	2565	
No. of parameters	154	
Weighting scheme	$w=1/[\sigma^2(F_0^2)+(0.0386P)^2+1.4477P]$, $P=(F_0^2+2F_c^2)/3$	
$\Delta\rho_{max}$, $\Delta\rho_{min}$ (e $Å^{-3}$)	0.461, -0.384	

2.4. Calculation Details

The molecular geometry of the compound is directly taken from the X-ray diffraction experimental result of the geometry optimization. This result was used at in the Gaussian 09 software package and the Gauss-view visualization program [37,38] for the DFT calculations with Becke's three-parameter Hybrid Functional Using the Lee-Yang-Parr (LYP) Correlation Functional B3LYP and PBE1PBE hybrid functional of Perdew, Burke and Ernzerhof which uses 25% exchange and 75% correlation weighting at LANL2DZ basis sets by using the Berny method [39-45]. The optimized structure parameters of the title

compound were calculated by using Hartree-Fock (HF) and density functional theory (DFT) with the functionals B3LYP and PBE1PBE using the base set LANL2DZ.

The Mulliken atomic charges and natural population analysis (NPA) for the included H atoms of the compound were calculated at LANL2DZ level by NBO analysis [46].

To compare the experimental (FT-IR) and calculated vibrational frequencies of the title compound, the vibrational frequency analyses revealed. It is well-known that the vibrational wavenumbers obtained by DFT computations usually overestimate than their experimental counterpart. These discrepancies can be corrected either by computing anharmonic corrections or by introducing a scaled field. In the calculations, made by the B3LYP/LANL2DZ level, the calculated vibrational wavenumbers were scaled by 0.9614 [47]. The assignments of each vibrational mode were defined from their potential energy distributions (PED) which were calculated by using VEDA 4 program based on B3LYP [48]. The visual check for the vibrational band assignments were also performed by using Gauss-View molecular visualization program.

3. RESULTS AND DISCUSSIONS

3.1. X-Ray Crystal Structure

The title compound $[(Hipb)_2].[PtCl_4]_2.H_2O$ is salt that consist of a square-planar tetrachloroplatinate(II) anion with hydrogen bonds to ring H atoms on two ($C_{10}H_{13}N_2$), (Hipb)+ cations and one water molecule in the structure. In the compound, the Pt atoms reside at a centre of inversion. The average Pt–Cl bond distance is 2.297(1) Å. The bond lengths at the Pt atom can be compared with that of 2.316(1) Å and 2.306(1) Å in $(Hhpb)_2.[PtCl_6]$ and $(Hhpb)_2{\cdot}[PtCl_4]$ [29], 2.314(1) Å in K_2PtCl_6 [49] and 2.323(4) Å in K_2PtCl_6 [50] and 2.324(4) Å in the $[PtCl_6]$ salt [51].

The structure of the investigated compound consists of discrete $(Hipb)^+$ cations and $[PtCl_4]^{2-}$ anions. In the compound, each $[PtCl_4]^{2-}$ anion is linked to two cations with hydrogen bonds N···Cl [3.249(4) from 3.660(7) Å], C···Cl [range from 3.553(7) to 3.895(7) Å]. There is a non-coordinating water molecule in the crystal structure. This molecule and the $(Hipb)^+$ cation and $[PtCl_4]^{2-}$ anions are linked *via* intermolecular hydrogen bonds N···O [2.728(8) Å], O···Cl [range from 3.234(6) to 3.451(7) Å], C···O [range from 3.350(7) to 3.545(1) Å]. The hydrogen-bonding interactions are summarized in Table 3 and visualized in Fig. 2 and Fig. 3. The crystal packing diagram for the investigated compound is shown in Fig. 3.

Table 2*. The experimental (X-ray) and optimized (HF, B3LYP and PBE1PBE /gas phase with LANL2DZ levels) geometric parameters of the title compound. Bond distances (Å) and angles (°) with estimated standard deviations (e.s.d.s) in parentheses.*

Parameters		LANL2DZ		
	Experimental	HF	B3LYP	PBE1PBE
Bond lengths (Å)				
N1–C7	1.328(6)	1.32582	1.37786	1.34265
N1–C6	1.389(6)	1.40280	1.40509	1.36094
N2–C7	1.330(6)	1.34465	1.36837	1.36094
N2–C1	1.389(6)	1.40763	1.41127	1.40269
C1–C6	1.384(7)	1.39237	1.41738	1.41125
C1–C2	1.386(7)	1.39003	1.40252	1.39742
C2–C3	1.370(9)	1.39079	1.40522	1.39925
C3–C4	1.389(9)	1.40865	1.42058	1.41514
C4–C5	1.370(9)	1.39000	1.40378	1.39791

C5–C6	1.390(7)	1.38984	1.40509	1.39678
C7–C8	1.493(7)	1.50671	1.50243	1.49294
C8–C10	1.523(7)	1.53784	1.54401	1.53380
C8–C9	1.524(8)	1.54776	1.55554	1.54450
Cl1–Pt1	2.296(1)	2.44874	2.44373	2.41596
Cl2–Pt1	2.298(1)	2.46308	2.44351	2.40791
Max. difference[a]		*0.16508* (Cl2 – Pt1)	*0.14773* (Cl1 – Pt1)	*0.11996* (Cl1 – Pt1)
RMSE[a]		*0.051933*	*0.043353*	*0.038332*
Bond angles (°)				
C7–N1–C6	109.3(4)	110.194	110.263	109.930
C6–C1–C2	121.8(5)	121.937	121.802	121.751
C6–C1–N2	105.5(4)	105.689	105.548	106.554
C2–C1–N2	132.7(5)	132.366	132.642	131.680
C3–C2–C1	116.3(5)	116.493	116.451	116.565
C2–C3–C4	121.9(5)	121.506	121.663	121.704
C5–C4–C3	122.4(5)	121.616	121.764	121.632
C4–C5–C6	115.8(5)	116.441	116.417	116.492
C1–C6–N1	106.8(4)	106.174	106.476	105.531
C1–C6–C5	121.8(5)	121.992	121.877	121.843
N1–C6–C5	131.4(5)	131.812	131.621	132.620
N1–C7–N2	108.5(4)	108.247	107.770	107.821
N1–C7–C8	124.5(4)	125.560	125.941	125.990
N2–C7–C8	127.0(4)	126.182	126.280	126.185
C7–C8–C10	110.1(4)	109.513	110.698	110.801
C7–C8–C9	112.5(4)	111.797	111.954	112.022
C10– C8– C9	111.0(5)	112.145	111.961	112.038
Cl1– Pt1–Cl1^{i}	180.00(6)	179.991	179.949	179.991
Cl2– Pt1–Cl2^{i}	180.00(5)	179.980	179.958	179.988
Cl1– Pt1–Cl2	89.64(5)	89.354	89.216	88.792
Cl1–Pt1–Cl2^{i}	90.641(5)	90.641	90.784	91.210
Max. difference[a]		*1.697*(C7–C8–C9)	*1.441*(N2–C7–C8)	*1.922* (C7–C8–C9)
RMSE		*1.025124*	*0.586708*	*1.002189*
Selected torsion angles (°)				
N1–C7–C8–C10	12.6(3)	9.392	9.426	8.746

N2–C7–C8–C9	66.2(2)	65.064	65.017	63.712
N1–C7–C8–C9	-111.8(2)	-116.270	-111.954	-117.172
N2–C7–C8–C10	-169.4(2)	-169.274	-169.297	-170.369
C2–C1–C6–N1	-179.6(2)	-179.986	-179.975	-177.982
C5–C6–C1–N2	-179.6(2)	-179.986	-177.463	-179.941
C6–N1–C7–C8	178.4(3)	178.136	177.616	178.617
C1–N2–C7–C8	178.2(3)	177.548	178.196	178.107

[a]*RMSE and maximum differences between the bond lengths and angles computed using theoretical methods and those obtained from X-ray diffraction.*
[i]*Symmetri code: (-x,-y,-z).*

The relative displacement of adjacent $(Hipb)^+$ cations is form an infinite chain structure with a trans-zigzag type along the crystallographic axis "*a*", through an intermolecular hydrogen bond. The interplanar spacing difference of $(Hipb)^+$ cations is 3.497 Å. The $(Hipb)^+$ is almost a planar molecule, but the methyl substituents (CH_3) deviates somewhat from that plane, where the dihedral angles T1 (N1-C7-C8-C10) and T2 (N2-C7-C8-C9) are 12.64(5) and 66.18(5)°.

In crystal structure of the title compound, there are two intramolecular hydrogen bonds and ten intermolecular hydrogen bonds. The donor and acceptor distances are 2.728(6) Å for N1–H1n···O1, 2.777(1) Å for C10–H10c···O1, 3.660(7) Å for N1–H1n···Cl1[i], 3.249(4) Å for N2–H2n···Cl1[i], 3.290(6) Å for O1–H1o···Cl1[v], 3.234(6) Å for O1–H2o···Cl2[vi], 3.451(6) Å for O1–H2o···Cl1[vi], 3.545(6) Å for C9–H9a···O1[ii], 3.503(8) Å for C10–H10c···O1[ii], 3.553(7) Å for C5–H5···Cl1[vi], 3.895(7) Å for C9–H9b···Cl2[iii], and 3.802(6) Å for C9–H9c···Cl1[ii] [Symmetry codes (i): *x,+y,+z+1*; (ii): *-x+1,-y+1,*-z;(iii): *-x,-y,-z+1*; (iv): *-x,-y+1,-z*; (v): *x+1,+y,+z*; (vi): *-x,-y,-z*], respectively. The details of the hydrogen bonds are summarized in Table 3.

Table 3. *Hydrogen-bond[a] geometry for the investigated compound.*

D–H···A (Atom)	D–H (Å)	H···A (Å)	D···A (Å)	D–H···A (°)
N1–H1n···Cl1[i]	0.86(1)	3.364(4)	3.660(7)	104.3(3)
N2–H2n···Cl1[i]	0.86(1)	2.424(1)	3.249(4)	161.1(3)
N1–H1n···O1	0.84(1)	1.898(4)	2.728(6)	169.0(3)
O1–H1o···Cl1[v]	0.87(1)	2.442(1)	3.290(6)	166.6(1)
O1–H2o···Cl2[vi]	0.86(1)	2.617(1)	3.234(6)	154.9(1)
O1–H2o···Cl1[vi]	0.86(1)	3.043(1)	3.451(6)	123.0(1)
C10–H10c···O1	0.960(1)	2.777(1)	3.350(9)	119.0(1)
C9–H9a···O1[ii]	0.960(1)	2.917(1)	3.545(6)	124.1(1)
C10–H10c···O1[ii]	0.960(1)	2.836(1)	3.503(8)	127.4(1)
C5–H5···Cl1[vi]	0.930(1)	3.233(2)	3.553(7)	102.5(4)
C9–H9b···Cl2[iii]	0.960(1)	2.957(2)	3.895(7)	165.8(4)
C9–H9c···Cl1[ii]	0.960(1)	2.922(1)	3.802(6)	153.0(4)

[a]*A= acceptor, D=donor atom.*
Symmetry codes (i): x,+y,+z+1; (ii): -x+1,-y+1,-z;(iii): -x,-y,-z+1; (iV): -x,-y+1,-z; (V): x+1,+y,+z; (vi): -x,-y,-z.

3.2. Optimized Molecular Structure

The molecular structure of the title compound $[(Hipb)_2].[PtCl_4]_2.H_2O$ has been experimentally determined. The optimized structure parameters such as bond lengths, bond angles, and dihedral angles of the title compound were calculated by using Hartree-Fock (HF) and density functional theory (DFT) with the functional B3LYP and PBE1PBE using the LANL2DZ basis set. The optimized molecular structures by using Hartree-Fock (HF), and the B3LYP functional (B3LYP and PBE1PBE) with LANL2DZ basis set can be seen from Figure 4a, 4b, and 4c. As seen from Table 2, when the X-ray structure of the title compound is compared with its optimized counterparts, conformational discrepancies are observed between them. It should be noted that the intermolecular interactions (Figure 3) in solid cisplatin lead to significant distortion of the $PtCl_2$. Therefore, the experimental results for solid cisplatin cannot serve as a rigorous check for the theoretical studies. In the Table 2, it is seen that the calculated Pt-Cl bond length for the title compound with HF, B3LYP and PBE1PBE at LANL2DZ basis set are 2.4559, 2.4436 and 2.4119 Å. In comparison with the same experimental value of 2.297(1) Å, the calculation results at HF, B3LYP and PBE1PBE at LANL2DZ levels are larger than experimental value, by 0.16508 Å for Cl2 – Pt1, 0.14773 Å for Cl1 – Pt1, and 0.11996 for Cl1 – Pt1. So, the PBE1PBE predicts the Pt – Cl bond length (2.4119 Å) in better agreement with experiment than all other functional. The calculated Cl–Pt–Cl angle varies in the range 88.79° (PBE1PBE) to 179.99° (HF), whereas the experimental values are vary 89.64(5)° to 180.00(6)°. The calculated values of Cl–Pt–Cl angles are smaller than those theoretically predicted for the free molecule. The most significant structural disparities are found in the orientation of the N1, C7, C8, and C10 atoms in the $(Hipb)^+$ cations. The torsion angle N1–C7–C8–C10 has been calculated as 9.392° for the HF, 9.426° for the B3LYP, and 8.746° for the PBE1PBE level, while the experimental value of the torsion angle N1–C7–C8–C10 is 12.6(3)°. As seen in Table 2, the B3LYP predicts the bond angles and torsion angles in better agreement with experiment than all other functional.

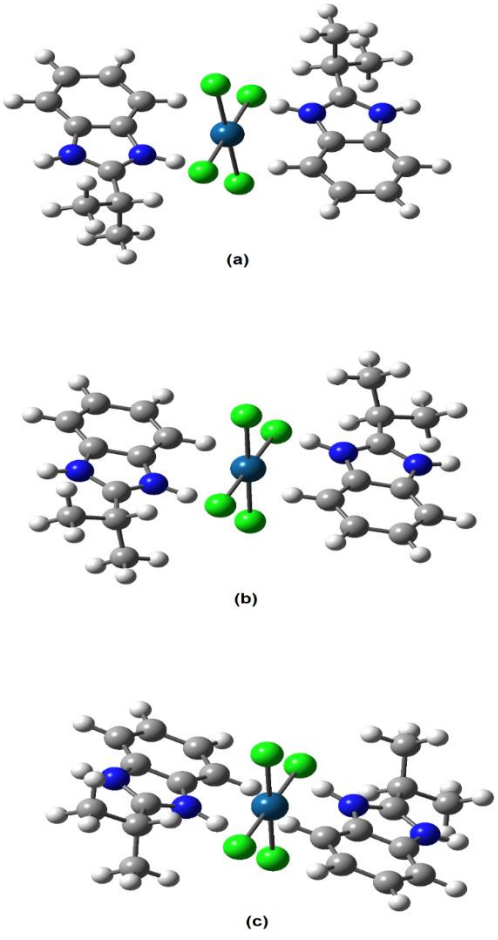

Figure 4. *The title compound's* ***(a)*** *Hartree-Fock (HF) optimized counterpart;* ***(b)*** *DFT (B3LYP) optimized counterpart;* ***(c)*** *DFT (PBE1PBE) optimized counterpart.*

It is well known that DFT-optimized bond lengths are usually longer and more accurate than HF due to the inclusion of electron correlation [52,53]. According to our calculations (Table 2), the biggest difference between experimental and calculated bond lengths is about 0.16508 Å (Cl2 – Pt1) for HF, 0.14773 Å (Cl1 – Pt1) for B3LYP level, while the root mean square error (RMSE) is found to be 0.051933 Å for HF, 0.043353 Å for B3LYP. For bond angles, as can be seen from Table 2, both the biggest difference and the RMSE obtained by the HF calculations (1.025124) are bigger than those determined by B3LYP (0.586708) level. According to these results, it may be concluded that the HF calculation well reproduces the bond lengths, while the B3LYP level is better at predicting the bond angles and 3D geometry of the title compound. We noted that the experimental results belong to the solid phase whereas theoretical calculations belong to the gas-phase. The result in the differences of bond parameters between the calculated and experimental values depend on the existence of the crystal field along with the inter-molecular interactions connects the molecules together in the solid state.

3.3. Vibrational Spectra

The vibrational band assignments were performed at B3LYP/LANL2DZ theory level defined from their potential energy distributions (PED) to compare the experimental (FT-IR) and calculated vibrational frequencies of the title compound (Figure 5). We have analyzed the normal vibrational frequencies and compared our calculated results of the investigated compound with the experimental ones on the basis of potential energy distributions (PED) and given in Table 4. The infrared spectra of the investigated compound have some characteristic bands of the vibrations of the N–H, C–H, C–H_3, C–N, C–C, and Pt–Cl groups.

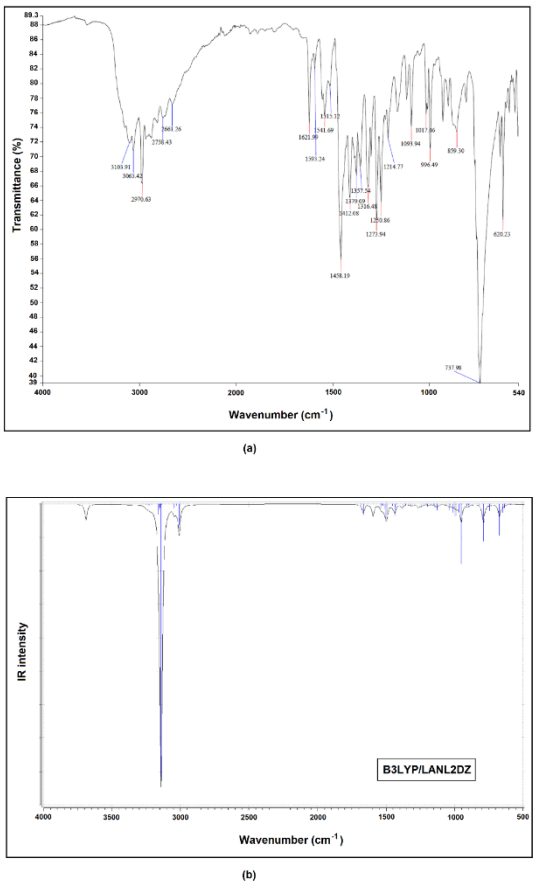

Figure 5. *Comparison of the experimental and calculated FT-IR spectra of the investigated compound:* ***(a)*** *Observed spectra;* ***(b)*** *Theoretical spectra at B3LYP/LANL2DZ level.*

***Table 4**. Comparison of the experimental and calculated vibrational frequencies (cm^{-1}).*

Experimental (FT-IR)	B3LYP/LANL2DZ Unscaled freq.	B3LYP/LANL2DZ Scaled freq.	Assignments Potential Energy Distributions (%PED)
3540	3688	3546	$\upsilon(NH)_{ring}(100)$
3104	3252	3126	$\upsilon_s(CH)_{ph}(97)$
3100	3223	3099	$\upsilon_{as}(CH)_{ph}(90)$
	3208	3084	$\upsilon_{as}(CH)_{ph}(100)$
	3161	3039	$\upsilon_{as}(CH_3)(71)+\upsilon(NH)_{ring}$ (29)
	3152	3030	$\upsilon_{as}(CH_3)(73)+\upsilon(NH)_{ring}$ (18)
	3150	3028	$\upsilon_{as}(CH_3)(13)+\upsilon(NH)_{ring}$ (85)
	3142	3021	$\upsilon_{as}(CH_3)(9)+\upsilon(NH)_{ring}$ (90)
	3140	3019	$\upsilon_{as}(CH_3)(49)$
2971	3113	2993	$\upsilon_{as}(CH_3)(100)$
2934	3046	2928	$\upsilon_s(CH_3)(92)$
	3030	2913	$\upsilon_s(CH_3)(56)+\upsilon(CH)(47)$
	3009	2893	$\upsilon(CH)(94)$
1622	1679	1614	$\upsilon(CC)_{ring}(53)$
1593	1666	1602	$\upsilon(CC)_{ring}(35)$
1542	1595	1533	$\upsilon(C7\text{-}C8)(51)+\delta(CH)_{ph}(33)$
	1534	1475	$\delta(CH_3)_{as}(38)+\delta(CH)_{ph}(46)$
1459	1523	1464	$\delta(CH_3)_{as}(70)$
	1502	1444	$\delta(CH_3)_{as}(18)+\delta(CH)(17)$
1412	1493	1435	$\delta(CH)_{ph}(34)$
	1453	1397	$\delta(CH_3)_s(umbrella)(53)$
1379	1437	1382	$\delta(CH_3)_s(umbrella)(45)$
1358	1419	1364	$\upsilon(CC)_{ring}(35)+\delta(CH)(15)+\delta(NH)(9)$
1317	1382	1329	$\upsilon(C\text{-}N)_{ring}(15)+\delta(NH)(24)+\delta(CH)(53)$
1302	1356	1304	$\gamma(CH)(45)$
1274	1315	1264	$\upsilon(C\text{-}N)_{ring}(33)+\upsilon(CC)_{ring}(27)+\delta(CH)_{ph}(11)$
1214	1268	1219	$\upsilon(C\text{-}N)_{ring}(11)$
	1246	1198	$\upsilon(C\text{-}N)_{ring}(10)$
1164	1204	1158	$\delta(CH)_{ph}(46)+\upsilon(CC)_{ring}(32)$
	1197	1151	$\gamma(CH_3)(30)$
1118	1150	1106	$\upsilon(C8\text{-}C9)(21)+\upsilon(C8\text{-}C10)(25)$
1094	1129	1085	$\gamma(CNC)_{ring}(10)+\tau(HCCC)(20)$
1010	1039	999	$\delta(CH)_{ph}(26)+\upsilon(CC)_{ring}(32)$
997	1030	990	$\tau(HCCC)_{ph}(68)$
	1014	975	$\gamma(NCC)_{ring}(26)$
	994	956	$\tau(HCCC)(21)$
	989	951	$\tau(HCCN)_{ring}(26)+\tau(HCCC)_{ph}(61)$

930	970	933	$\rho(CH_3)(25)$
	951	914	$\gamma(NH)(26)$
	911	876	$\upsilon(CC)_{ring}(58)+\upsilon(C\text{-}N)_{ring}(25)$
859	898	863	$\upsilon(C8\text{-}C9)(36)+\upsilon(C8\text{-}C10)(14)$
767	790	760	$\tau(HCCC)_{ph}(68)$
739	783	753	$\tau(CCCC)_{ph}(12)+\tau(NCCC)_{ring}(61)$
	745	716	$\upsilon(C7\text{-}C8)(17)+\tau(C7NCC)(13)$
635	674	648	$\gamma(NH)(87)$
603	636	611	$\upsilon(CC)_{ring}(45)$
570	590	567	$\tau(CCCC)_{ph}(69)$
	499		$\delta(CCC)_{ph}(13)+\delta(C7C8N)_{ph}(14)+$
		480	$\gamma(C10C9C8C7)(16)$
	457	439	$\gamma(NCCC)_{ph}(39)$
	414	398	$\tau(CNCC)_{ring}(18)+\tau(CCCC)_{ph}(18)+\gamma(C9C8C7)(21)$
	320	308	$\upsilon_a(PtCl)(97)$
	306	294	$\upsilon_s(PtCl)(90)$

v: bond stretching, δ: in-plane angle bending, γ: out-of-plane angle bending, ρ: rocking, τ: torsion, as: antisymmetric and s: symmetric.

N–H vibrations

The N–H stretching vibrations give rise to bands at about 3500–3200 cm^{-1} [54]. In the present study, the bands observed at 3540 cm^{-1} in the IR spectrum, and 3546, 3039, 3030, 3028 and 3021 cm^{-1} (B3LYP) were assigned as N–H stretching vibration with 100, 29, 85 and 90% contribution of PEDs. The N–H group shows bands at 1510–1500, 1350–1250 and 740–730 cm^{-1} [55]. According to literature, if the N–H is a part of a closed ring, the C–N–H deformation band is absent in the region 1510–1500 cm^{-1} [55,56]. For the title compound, the C–N–H deformation band is observed at 1358 and 1317 cm^{-1} in the FT-IR spectrum and at 1364 and 1329 cm^{-1} theoretically (B3LYP) assigned. The out of plane N–H deformation is expected in the region 650±50 cm^{-1} [56]. The experimental out of plane N–H deformation is observed at 635 cm^{-1} and calculated at 648 cm^{-1} with 87% contribution of PEDs (B3LYP).

C–H vibrations

The aromatic structure shows the presence of C–H stretching vibrations in the region 3000 – 3125 cm^{-1}, which is the characteristic region for the identification of υ(CH) stretching vibrations. But in this region, the bands are not appreciably affected by the nature of the substituent [57]. The observed the asymmetric C–H stretching vibration is 3100 cm^{-1}, while the calculated values the asymmetric C–H stretching vibrations are 3099, and 3084 cm^{-1} with the 90 and 100% contribution of PEDs. The symmetric C–H stretching vibration is observed at 3104 cm^{-1}. The B3LYP calculations give this mode at the 3126 cm^{-1} with the 97% contribution of PED. Substitution sensitive C–H in-plane bending vibrations lie in the region 1000–1300 cm^{-1} [58]. In the compound, infrared bands range 1274, 1164, and 1010 cm^{-1} are assigned to C–H in-plane bending vibrations. These vibrations are corresponding to 1264, 1158, and 999 cm^{-1} of calculated values.

C–H₃ vibrations

The $\upsilon_s(CH_3)$-symmetric stretching, $\upsilon_{as}(CH_3)$-asymmetric stretching, $\delta(CH_3)_s$-symmetric bending deformation, and $\delta(CH_3)_{as}$-asymmetric bending deformation frequencies are assigned for the CH_3 group in the investigated compound. The $\upsilon_{as}(CH_3)$- asymmetric stretching vibration is generally observed at the 2962±10 cm^{-1}, while the $\upsilon_s(CH_3)$-symmetric stretching will appear 2872±10 cm^{-1} [54]. The $\upsilon_s(CH_3)$-symmetric stretching vibration is observed at 2934 cm^{-1}, and assigned at 2928 and 2913 cm^{-1} by B3LYP. The $\upsilon_{as}(CH_3)$-asymmetric stretching modes is observed at 2971 cm^{-1}. The B3LYP calculations give this

mode in the range 2993-3039 cm^{-1}. The $\delta(CH_3)_s$-bending deformation (umbrella mode) show up at 1375±10 cm^{-1}, while $\delta(CH_3)_{as}$-asymmetric bending deformation show up at 1460±10 cm^{-1} [54]. In our present study, the $\delta(CH_3)_s$-bending deformation (umbrella mode) vibrations are assigned at 1397, and 1382 cm^{-1}, whereas $\delta(CH_3)_{as}$-asymmetric bending deformation modes are assigned at 1475, 1464, and 1444 cm^{-1}. The $\delta(CH_3)_{as}$-asymmetric bending deformation and $\delta(CH_3)_{as}$-symmetric bending deformation are observed at 1459 cm^{-1} and 1379 cm^{-1} as experimentally.

C–N vibrations

The C–N stretching modes are expected in the range 1100–1300 cm^{-1} [53]. The bands observed at 1317, 1274, and 1214 cm^{-1} in the IR spectrum and at 1329, 1264, 1219, and 1198 cm^{-1} theoretically (B3LYP) are assigned as C–N stretching modes.

C–C and C=C vibrations

The ring C=C stretching vibrations for aromatic group generally appear 1430-1625 cm^{-1} [59] and usually assigned to C=C stretching modes in 1400-1650 cm^{-1} [60]. For title compound, the C–C and C=C stretching vibrations are observed at 1622, and 1593 cm^{-1} in FT-IR spectrum. The B3LYP calculations give these modes at the 1614, and 1602 cm^{-1}. The mean difference between theoretical and experimental frequencies is about 8 cm^{-1}. It shows the good agreement between theoretical and experimental the ring C–C and C=C stretching vibrations for aromatic group.

Pt–Cl vibrations

For cis-complexes infrared active stretching vibrations are depend on nature of the ligand, the Pt–Cl stretching vibration υ(PtCl) occurring in the ranges, 343-302 cm^{-1}, and 328-281 cm^{-1} [61]. The υ(PtCl) stretching vibrations are calculated at 308 and 294 cm^{-1} with pure modes, the 90 and 97 % contribution of PEDs by B3LYP level.

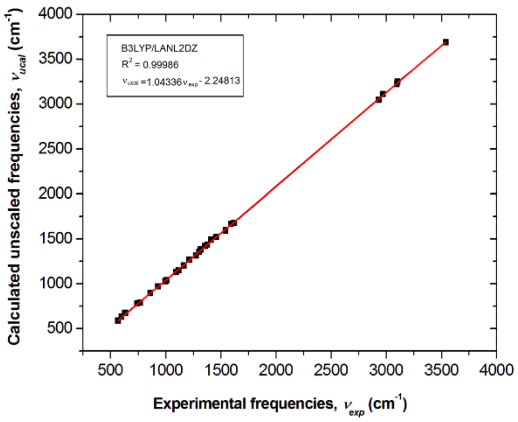

Figure 6. *Correlation graphics of unscaled (calculated) and experimental frequencies of the title compound.*

The calculated values of other group vibrations show good agreement with the experimental results. The other experimental and calculated vibrational values can be seen in Table 4. To make a comparison with the experimental observation, we present correlation graphics in Figure 6. The relation between the calculated unscaled (ν_{ucal}) and experimental (ν_{exp}) wavenumbers is linear and described by the following equation:

$$\nu_{ucal} = 1.04336\nu_{exp} - 2.24813, \quad R^2 = 0.99986 \tag{1}$$

According to the fitting results of the equation (1), the general scale factor value was found to be 0.958 for B3LYP/LANL2DZ. As a result, the scaled fundamental vibrationals are in good consistency with experimental results and are found a good agreement above the predicted literature.

3.4. Atomic Charge Distributions and Dipole Moment Behavior

The calculation of atomic charges plays a significant role in the application of quantum mechanical calculations to molecular systems because of atomic charges affect some properties of molecular systems including dipole moment and molecular polarizability. The atomic charges have been also used to describe the MEP surfaces [53,62,63]. The both Mulliken's atomic net charges [46] and the natural population analysis (NPA) atomic charges [64] were calculated using B3LYP/LANL2DZ and listed in Table 5. The calculated Mulliken and NPA atomic charges for gas phase were illustrated in Figure 7. According to the calculated Mulliken atomic charges and, the C7 (and $C7^{i}$) atom has a largest positive atomic charge and C9 (and $C9^{i}$) atom has a largest negative atomic charge. As can be seen in Figure 7 and Table 5, all of the hydrogen atoms have net positive charge. The obtained atomic charge was showed that the H1n and H2n atoms have bigger positive atomic charge than the other hydrogen atoms, while the imine N1 and N2 atoms have negative atomic charge. The Pt atom has a large negative atomic charge in the gas phase, respectively. These behaviors may be result of the intermolecular N–H···Pt hydrogen bond. As seen from Table 5, the Mulliken and charge value of Pt is -0.467008, respectively, being lower than the formal charge -2. It is a consequence of charge donation from the two $(Hipb)^{+}$. According to these results, the remarkable differences between the calculated Mulliken and NPA atomic charges for gas phase are due to the different theoretical background. The NPA satisfies Pauli's exclusion principle and is regarded as more important compared to the Mulliken population analysis, which shows great variations depending on the type of base sets.

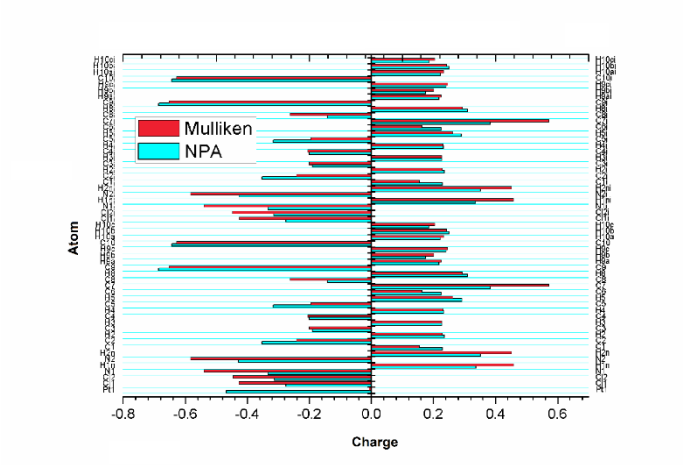

Figure 7. *The Mulliken and NPA atomic charge distribution of the compound in the gas phases.*

Table 5. *Calculated net charges by Mulliken population method and natural population analysis (NPA) in gas phase.*

B3LYP/LANL2DZ		
Atom	Mulliken charges	NPA natural charges
Pt1	-0.467008	-0.00757
Cl1	-0.275323	-0.42645
Cl2	-0.312903	-0.44688
N1	-0.333096	-0.53935
H1n	0.337187	0.45809
N2	-0.427625	-0.58443
H2n	0.351595	0.45079

C1	0.228972	0.153970
C2	-0.352802	-0.24136
H2	0.234697	0.22784
C3	-0.189437	-0.20153
H3	0.227514	0.22704
C4	-0.201570	-0.20452
H4	0.233026	0.23054
C5	-0.316051	-0.19530
H5	0.291506	0.26162
C6	0.225798	0.16226
C7	0.383324	0.57191
C8	-0.142057	-0.26257
H8	0.309544	0.29343
C9	-0.687007	-0.65325
H9a	0.218085	0.22494
H9b	0.175132	0.20121
H9c	0.240954	0.24580
C10	-0.644190	-0.62850
H10a	0.222068	0.23202
H10b	0.250793	0.24258
H10c	0.185218	0.20391
$Cl1^{i}$	-0.274927	-0.42605
$Cl2^{i}$	-0.313594	-0.44731
N1i	-0.332833	-0.53941
$H1n^{i}$	0.336678	0.45800
N2i	-0.427553	-0.58444
$H2n^{i}$	0.351704	0.45083
$C1^{i}$	0.229172	0.15401
$C2^{i}$	-0.352801	-0.24121
$H2^{i}$	0.234752	0.22788
$C3^{i}$	-0.189575	-0.20162
$H3^{i}$	0.227534	0.22704
$C4^{i}$	-0.201275	-0.20462
$H4^{i}$	0.232831	0.23043
$C5^{i}$	-0.316060	-0.19541
$H5^{i}$	0.290496	0.26108
$C6^{i}$	0.225629	0.16242

$C7^i$	0.383947	0.57217
$C8^i$	-0.141900	-0.26229
$H8^i$	0.310138	0.29329
$C9^i$	-0.687175	-0.65327
$H9a^i$	0.218033	0.22491
$H9b^i$	0.174999	0.20113
$H9c^i$	0.241331	0.24602
$C10^i$	-0.644211	-0.62849
$H10a^i$	0.222568	0.23232
$H10b^i$	0.250750	0.24258
$H10c^i$	0.185001	0.20379

The dipole moments of the compound calculated using B3LYP/LANL2DZ level. Dipole moment in a molecule can be used as an indicator of the charge movement across the molecule. The direction of the dipole moment depends on the positive and negative charge centers. As our calculated results, the maximum contribution to the dipole moment is from *y* direction (0.0693882 D), whereas the contribution of *z* direction to the dipole moment is negligible (0.0030359). The calculated value of total dipole moment is 0.1778 D for the compound.

3.5. Molecular Electrostatic Potential Surface

To investigate reactive sites for electrophilic and nucleophilic attack, the regions of the MEP for the title compound was composed by DFT calculation using the optimized geometry at the B3LYP/LANL2DZ. As shown Figure 8, red and yellow colors indicated for the negative regions of the MEP are related to electrophilic reactivity, while blue colors indicated for positive regions to nucleophilic reactivity. As can be seen from Figure 7, the compound has four possible sites for electrophilic attack. The chlorine atoms Cl1, Cl2, Cl3, Cl4 have negative region. The negative molecular electrostatic potential region is varies at 0.065 – 0.039 a.u. on the Chlorine atoms. The H1n atoms of the N1 have positive region to nucleophilic attack with a maximum value (0.089 a.u). According to these calculated results, the region of MEP shows that the negative potential sites are on electronegative atoms as well as the positive potential sites are around the hydrogen atoms. The determining of MEP region is best suit for identifying sites for intra- and intermolecular interactions [65]. According to the MEP surface of the compound, the weak negative region associated with chlorine atoms and also the weak positive region by the nearby H1n atoms. It can be indicative of an intermolecular (Cl–H1n···N) hydrogen bonding in the compound.

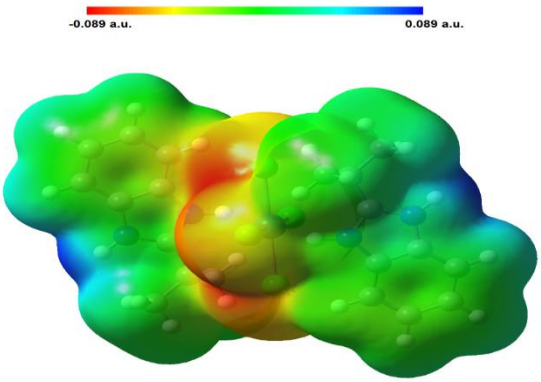

Figure 8. *Molecular electrostatic potential (MEP) map calculated at B3LYP/LANL2DZ level (the isodensity values ±0.089 a.u).*

3.6. The HOMOs –LUMOs Orbitals

The highest occupied molecular orbital (HOMO) and the lowest unoccupied molecular orbital (LUMO), which named the frontier molecular orbitals are the very important parameters for quantum chemistry. The frontier molecular orbitals play an important role in the electric properties and determine the way the molecule interacts with other species [66,67]. Figure 9 presents the distribution and energy band gaps of HOMO-1, HOMO, LUMO, LUMO+1 orbitals computing at B3LYP/LANL2DZ level for the title compound.

The HOMO and HOMO-1 orbitals of the compound are composed of the $d_{x^2-y^2}$ molecular orbital of Pt(II), whereas the LUMO and LUMO+1 orbitals of the compound are composed of the π molecular orbital of the $[(Hipb)_2]^+$ ligand, as seen in Figure 9. Except for ethoxy group atoms in the $[(Hipb)_2]^+$ ligand, the LUMOs are mainly localized on the whole structure.

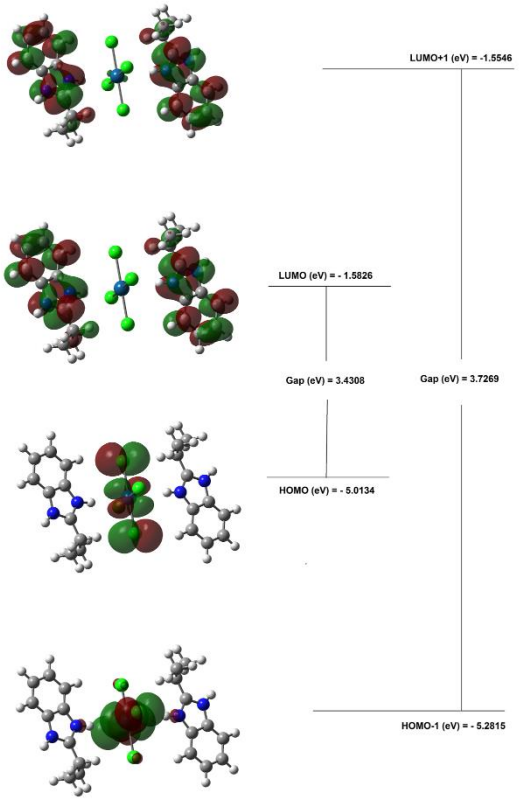

Figure 9. *Molecular orbital surfaces and energy levels for the HOMO, HOMO-1, LUMO, and LUMO+1 of the title compound computed at B3LYP/LANL2DZ level.*

4. CONCLUSION

The 2-isopropylbenzimidazolium tetrachlroplatinate monohydrate $(C_{10}H_{13}N_2)_2.[PtCl_4].H_2O$ was prepared and characterized by using single crystal X-ray crystallographic characterization and spectroscopic methods. The X-ray structure analysis which showed $(C_{10}H_{13}N_2)_2.[PtCl_4].H_2O$ was salt that consist of a square-planar tetrachloroplatinate(II) anion, and Pt atoms reside at a center of inversion. The compound was comprised of 2-isopropylbenzimidazole $(Hipb)^+$: $(C_{10}H_{13}N_2)^+$ and $[PtCl_4]^{2-}$ ions , linked by intermolecular hydrogen bonds.

The computational models, Hartree-Fock (HF) and density functional theory (DFT), B3LYP and PBE1PBE functional with LANL2DZ basis set, provided good reproducibility of calculated bond distances and bond angles when compared with the experimental x-ray structure of the compound. Comparison of calculated IR spectra of the compound with the experimental ones allowed assignation of the most characteristic

modes. In addition, Mulliken's atomic net charges and the natural population analysis (NPA) atomic charges were calculated using B3LYP/LANL2DZ. The regions of the MEP for the title compound were composed by DFT calculation using the optimized geometry at the B3LYP/LANL2DZ to investigate reactive sites for electrophilic and nucleophilic attack. Finally, the distribution and energy band gaps of HOMO-1, HOMO, LUMO, LUMO+1 orbitals computing at B3LYP/LANL2DZ level for the title compound were revealed. The frontier molecular orbitals show $d_{x^2-y^2}$ molecular orbital for Pt(II), and π molecular orbital for the $[(Hipb)_2]^+$ ligand characteristic. The HOMO-LUMO energy gap value was found to be 3.4308 eV at B3LYP/LANL2DZ level.

In summary, this study is a combination of the theoretical and experimental characterizations on the platinum salt 2-isopropylbenzimidazolium tetrachlroplatinate monohydrate $(C_{10}H_{13}N_2)_2.[PtCl_4].H_2O$, the concept that already proved to be very useful in coordination and computational chemistry.

APPENDIX A. SUPPLEMENTARY MATERIAL

Supplementary data associated with this article can be found, in the online version, at http://dx.doi.org/

Note

1. Further information may be obtained from: Cambridge Crystallographic Data Center (CCDC), 12 Union Road, Cambridge CB21EZ, UK, by quoting the depository number CCDC 1044156, e-mail: deposit@ccdc.cam. ac.uk.

CONFLICT OF INTEREST

No conflict of interest was declared by the authors

REFERENCES

[1] Denny, W.A., Rewcastle, G.W. and Baguley, B.C., "Potential antitumor agents; structure-activity-relationships for 2-phenylbenzimidazole-4-carboxamides, a new class of minimal DNA-intercalating agents which may not act via topoisomerase-II", J. Med. Chem., 33(2): 814-819, (1990).

[2] Gravatt, G.L., Baguley, B.C., Wilson, W.R. and Denny, W.A., "Na-directed alkylating-agents; synthesis and antitumor-activity of DNA minor groove-targeted aniline mustard analogs of pibenzimol (Hoechst-33258)", J. Med. Chem., 37(25): 4338-4345, (1994).

[3] Kim, J.S., Gatto, B., Yu, C., Liu, A., Liu, L.F. and LaVoie, E.J., "Substituted 2,5'-bi-1H-benzimidazoles: Topoisomerase I inhibition and cytotoxicity", J. Med. Chem., 39(4):992-998, (1996)

[4] Horton, D.A., Bourne, G.T. and Smythe, M.L., "The combinatorial synthesis of bicyclic privileged structures or privileged substructures", Chem. Rev., 103(3): 893-930, (2003).

[5] Bradshaw, T.D., Wrigley, S., Shi, D.F., Schultz, R.J., Paull, K.D. and Stevens, M.F.G., "2-(4-aminophenyl)benzothiazoles: novel agents with selective profiles of in vitro anti-tumour activity", Brit. J. Cancer., 77(5): 745-752, (1998).

[6] Payne, J.E., Bonnefous, C., Symons, K.T., Nquyen, P.M., Sablad, M., Rozenkrants, N., Zhang, Y., Wang, L., Wang, L., Yazdani, N., Shiau, A.K., Noble, S.A., Rix, P., Rao, T.S., Hassiq, C.A. and Smith, N.D., "Discovery of dual inducible/neuronal nitric oxide synthase (iNOS/nNOS) inhibitor development candidate 4-(2-cyclobutyl-1H-imidazo[4,5-b]pyrazin-1-yl)methyl)-7,8-difluoroquinolin-2(1H)-one (KD7332) Part 2: Identification of a novel, potent, and selective series of benzimidazole-quinolinone iNOS/nNOS dimerization inhibitors that are orally active in pain models", J. Med. Chem., 53(21): 7739-7755, (2010).

[7] Roth, T., Morningstar, M.L., Boyer, P.L., Hughes, S.H., Buckheit, R.W. and Michejda, C.J., "Synthesis and biological activity of novel nonnucleoside inhibitors of HIV-1 reverse transcriptase. 2-aryl-substituted benzimidazoles", J. Med. Chem., 40(26): 4199-4207, (1997).

[8] Galal, S.A., Hegab, K.H., Kassab, A.S., Rodriguez, M. L., Kerwin, S.M., El-Khamry, A.A. and El Diwani, H.I., "New transition metal ion complexes with benzimidazole-5-carboxylic acid hydrazides with antitumor activity", Eur. J. Med. Chem., 44(4): 1500-1508, (2009).

[9] Wang, X.L., Hou, L.L., Zhang, J.W., Gong, C.H. and Liu, G.C., "Bis(benzimidazole)-based ligands-directed the various dimensionality of metal-organic complexes based on carboxylates co-ligands: Syntheses, structures and properties", Inorg. Chim. Acta., 405: 58-64, (2013).

[10] Abdel-Ghani, N.T., E-Ghar, M.F.A. and Mansour, A.M., "Novel Ni(II) and Zn(II) complexes coordinated by 2-arylaminomethyl-1H-benzimidazole: Molecular structures, spectral, DFT studies and evaluation of biological activity", Spectrochim Acta A, 104: 134-142, (2013).

[11] Arjmand, F., Parveen, S., Afzal, M. and Shahid, M., "Synthesis, characterization, biological studies (DNA binding, cleavage, antibacterial and topoisomerase I) and molecular docking of copper(II) benzimidazole complexes", J. Photoch. Photobio. B, 114: 15-26, (2012).

[12] Nicolini, M. (ed.), "Platinum and other metal coordination compounds in cancer chemotherapy: clinical application of platinum complexes", Martinus Nijhoff Publishing, Boston, (1988).

[13] Krause-Heuer, A.M., Grunert, R., Kuhne, S., Buczkowska, M., Wheate, N.J., Le Pevelen, D.D., Boag, L.R., Fisher, D.M., Kasparkova, J., Malina, J., Bednarski, P.J., Brabec, V. and Aldrich-Wright, J.R., "Studies of the mechanism of action of platinum(II) complexes with potent cytotoxicity in human cancer cells", J. Med. Chem., 52(17): 5474-5484, (2009).

[14] Johnstone, T.C., Wilson, J.J. and Lippard, S.J. "Monofunctional and higher-valent platinum anticancer agents", Inorg. Chem., 52(21): 12234-12249, (2013).

[15] Fraval, H.N.A. and Roberts, J.J., "Excision repair of cis-diamminedichloroplatinum(II)-induced damage to DNA of Chinese-Hamster cells", Cancer Res., 39(5): 1793-1797, (1979).

[16] Pinto, A.L. and Lippard, S.J., "Sequence-dependent termination of invitro DNA-synthesis by cis-diamminedichloroplatinum(II) and trans-diamminedichloroplatinum(II)", P. Natl. Acad. Sci. USA, 82(14): 4616-4619, (1985).

[17] Jamieson, E.R. and Lippard, S.J., "Structure, recognition, and processing of cisplatin-DNA adducts", Chem. Rev., 99(9): 2467-2498, (1999).

[18] Cleare, M.J., Hydes, P.C., Malerbi, B.W. and Watkins, D.M., "Anti-tumour platinum complexes - relationships between chemical properties and activity", Biochimie, 60(9): 835-850, (1978).

[19] Bloemink, M.J., Engelking, H., Karentzopoulos, S., Krebs, B. and Reedijk, J., "Synthesis, crystal structure, antitumor activity, and DNA-binding properties of the new active platinum compound (bis(N-methylimidazol-2-yl)carbinol)dichloroplatinum(II), lacking a NH moiety, and of the inactive analog dichloro(N-1, N-1'-dimethyl-2,2'-biimidazole)platinum(II)", Inorg. Chem., 35(3): 619-627, (1996).

[20] Domnina, E.S., Voropaev, V.N., Skvortsova, G.G., Minakova, S.M. and Chernov, V.A., "Synthesis and anti-tumoral activity of complex-compounds Pt(II), Pt(IV) and Pd(II) with 1-vinylazoles", Khim. Farm. Zh+, 17(6): 700-703, (1983).

[21] Gumus, F. and Algul, O., "DNA binding studies with cis-dichlorobis (5(6)-non/chlorosubstituted-2-hydroxymethyl-benzimidazole) platinum(II) complexes", J. Inorg. Biochem., 68(1): 71-74, (1997).

[22] Muir, M.M., Cox, O., Rivera, L.A., Cadiz, M.E. and Medina, E., "Synthesis and characterization of new platinum(II) complexes containing thiazole and imidazole donors dichlorobis(styrylbenzazole)platinum(II) complexes", Inorg. Chim. Acta., 191(1):131-139, (1992).

[23] Mylonas, S., Valavanidis, A., Dimitropoulos, K., Polissiou, M., Tsiftsoglou, A.S. and Vizirianakis, I.S., "Synthesis, molecular-structure determination, and antitumor-activity of platinum(II) and palladium(II) complexes of 2-substituted benzimidazole", J. Inorg. Biochem., 34(4): 265-275, (1988).

[24] Gumus, F., Algul, O., Eren, G., Eroğlu, H., Diril, N., Gür, S. and Ozkul, A., "Synthesis, cytotoxic activity on MCF-7 cell line and mutagenic activity of platinum(II) complexes with 2-substituted benzimidazole ligands", Eur. J. Med. Chem., 38(5):473-480, (2003).

[25] Gumus, F., Demirci, A.B., Ozden, T., Eroglu, H. and Diril, N. "Synthesis, characterization and mutagenicity of new cis-[Pt(2-substituted-benzimidazole)(2)Cl-2] complexes", Pharmazie, 58(5): 303-307, (2003).

[26] Gumus, F., Eren, G., Acik, L., Çelebi, A., Öztürk, F., Yılmaz, Ş., Ilıkçı Sağkan, R., Gür, S., Özkul, A., Elmalı, A.and Elerman, Y., "Synthesis, cytotoxicity, and DNA interactions of new cisplatin analogues containing substituted benzimidazole ligands", J. Med. Chem., 52(5): 1345-1357, (2009).

[27] Gumus, F., Pamuk, I., Ozden, T., Yıldız, S., Diril, N., Öksüzoğlu, E., Gür, S. and Özkul, A., "Synthesis, characterization and in vitro cytotoxic, mutagenic and antimicrobial activity of platinum(II) complexes with substituted benzimidazole ligands", J. Inorg. Biochem., 94(3): 255-262, (2003).

[28] Utku, S., Gumus, F., Tezcan, S., Serin, M.S. and Ozkul, A., "Synthesis, characterization, cytotoxicity, and DNA binding of some new platinum(II) and platinum(IV) complexes with benzimidazole ligands", J. Enzym. Inhib. Med. Chem., 25(4): 502-508, (2010).

[29] Elmali, A., Elerman, Y., Eren, G., Gumus, F. and Svoboda, I. "The crystal structures of 2-(3 '-hydroxypropyl)benzimidazolium hexa- and tetrachloroplatinate", Z. Naturforsch. B, 60(2): 164-168, (2005).

[30] Kukushkin, Y.N., Sedova, G.N., Khamnuev, G.K. and Garnovskii, A.D., "Thermal-Conversions of Platinum(Ii) Halide-Complexes with Imidazoles in Solid-Phase", Zh. Neorg. Khim., 26(3): 696-701, (1981).

[31] Kukushkin, Y.N., Vrublevskaya, L.V., Vlasova, R.A., Isachkina, T.S., Postnikova, E.S. and Sheleshkova, N.K., "Thermal solid-phase transformation of onium-type platinum(II) and palladium(II) rhodanide complexes", Zh Neorg Khim., 30(2): 401-406, (1985).

[32] Chari, M.A., Shobha, D., Sasaki, T., "Room temperature synthesis of benzimidazole derivatives using reusable cobalt hydroxide (II) and cobalt oxide (II) as efficient solid catalysts", Tetrahedron Lett., 52(43): 5575-5580, (2011).

[33] Bruker, APEX2, SAINT and SADABS. Bruker AXS, Inc. Madison, Wisconsin, USA, (2012).

[34] Sheldrick GM, SHELXS–97, "Program for the solution of crystal structures", Univ. of Goettingen, Germany, (1997).

[35] Sheldrick GM, SHELXL–97, "Program for the refinement of crystal structures", Univ. of Goettingen, Germany, (1997).

[36] Farrugia, L.J., "ORTEP-3 for Windows - a version of ORTEP-III with a Graphical User Interface (GUI)", J. Appl. Crystallogr. 30, 565, (1997).

[37] Dennington, R., Keith, T. and Millam, J.I., GaussView, Version 5. Semichem, Inc., Shawnee Mission, KS, (2009).

[38] Frisch, M. J., Trucks, G. W., Schlegel, H. B., et al. Gaussian 09, Revision D.01. Gaussian, Inc., Wallingford CT, (2009).

[39] Becke, A.D., "Density-functional thermochemistry; A new dynamical correlation functional and implications for exact-exchange mixing", J. Chem. Phys., 104(3): 1040-1046, (1996).

[40] Binning, R.C., Curtiss, L.A., "Compact contracted basis-sets for 3rd-row atoms - Ga-Kr", J. Comput. Chem., 11(10): 1206-1216, (1990).

[41] Dunning, Jr. T.H., Hay, P. J., "Modern Theoretical Chemistry", Vol. 3, Plenum, New York, (1977).

[42] Perdew, J.P., Burke, K., Ernzerhof, M., "Generalized gradient approximation made simple", Phys. Rev. Lett., 77(18): 3865-3868, (1996).

[43] Perdew, J.P., Burke, K., Ernzerhof, M., "Generalized gradient approximation made simple (vol 77, pg 3865, 1996)", Phys. Rev. Lett., 78(7): 1396-1396, (1997).

[44] Perdew, J.P., Kurth, S., Zupan, A., Blaha, P., "Accurate density functional with correct formal properties: A step beyond the generalized gradient approximation", Phys. Rev. Lett., 82(12): 2544-2547, (1999).

[45] Perdew, J.P., Kurth, S., Zupan, A., Blaha, P., "Accurate density functional with correct formal properties: A step beyond the generalized gradient approximation (vol. 82, Pg. 2544, 1999)", Phys. Rev. Lett., 82(25): 5179-5179, (1999).

[46] Mulliken, R.S., "Electronic population analysis on Lcao-Mo molecular wave functions", J. Chem. Phys., 23(10): 1833-1840, (1955).

[47] Perdew, J.P., Chevary, J.A., Vosko, S.H., Jackson, K.A., Pederson, M.R., Singh, D.J. and Fiolhais, C., "Atoms, molecules, solids, and surfaces - applications of the generalized gradient approximation for exchange and correlation (Vol 46, Pg 6671, 1992)", Phys. Rev. B, 48(7): 4978-4978, (1993).

[48] Merrick, J.P., Moran, D. and Radom, L., "An evaluation of harmonic vibrational frequency scale factors", J. Phys. Chem. A, 111(45): 11683-11700, (2007).

[49] Ohba, S. and Saito, Y., "Electron-density distribution in crystals of potassium hexachloroplatinate(IV), K2[PtCl6]", Acta. Crystallogr. C, 40(Oct): 1639-1641, (1984).

[50] Rau, F., Klement, U. and Range, K.J., "Crystal-structure of oxonium hexachloroplatinate(IV), (H3O)(2)PtCl6", Z. Kristallogr., 210(9): 684-684, (1995).

[51] Valle, G. and Ettorre, R., "Bis(2-chloro-1H-imidazol-3-ium)hexachloroplatinate(IV), (C3H4ClN2)(2)[PtCl6]", Acta. Crystallogr. C, 54: 448-449, (1998).

[52] Zeyrek, C.T., Dilek, N., Yildiz, M. and Unver, H., "Synthesis, structure, spectroscopic (FT-IR) and density functional modelling studies of 1-[(4-ethoxyphenylimino)methyl]napthalene-2-ol", Mol. Phys., 112(19): 2557-2574, (2014).

[53] Zeyrek, C.T., Unver, H., Arpaci, O.T., Polat, K., Iskeleli, N.O. and Yildiz, M., "Experimental and theoretical characterization of the 2-(4-bromobenzyl)-5-ethylsulphonyl-1,3-benzoxazole", J. Mol. Struct., 1081: 22-37, (2015).

[54] Smith, B.C., "Infrared spectral interpretation, a systematic approach", CRC Press, New York, (1999).

[55] Socrates, G., "Infrared characteristic group frequencies", John Wiley and Sons, New York, (1981).

[56] Roeges, N.P.G., "A guide to the complete interpretation of IR spectra of organic compounds", Wiley, New York, (1994).

[57] Teimouri, A., Chermahini, A.N., Taban, K. and Dabbagh, H.A., "Experimental and CIS, TD-DFT, ab initio calculations of visible spectra and the vibrational frequencies of sulfonyl azide-azoic dyes", Spectrochim. Acta. A, 72(2):369-377, (2009).

[58] Arunagiri, C., Subashini, A., Saranya, M., Muthiah, P.T., Thanigaimani, K. and Razak, I.A., "Synthesis, crystal structure and theoretical studies of a Schiff base 2-[4-hydroxy benzylidene]-amino naphthalene", Spectrochim. Acta. A, 135: 307-316, (2015).

[59] Govindarajan, M., Periandy, S. and Carthigayen, K., "FT-IR and FT-Raman spectra, thermo dynamical behavior, HOMO and LUMO, UV, NLO properties, computed frequency estimation analysis and electronic structure calculations on alpha-bromotoluene", Spectrochim. Acta. A, 97: 411-422, (2012).

[60] Michalska, D., Bienko, D.C., AbkowiczBienko, A.J., Latajka, Z., "Density functional, Hartree-Fock, and MP2 studies on the vibrational spectrum of phenol", J. Phys. Chem-Us, 100(45): 17786-17790, (1996).

[61] Ridley, D., "Synthetic and spectroscopic studies on some inorganic and organometallic compounds", PhD. Thesis, Durham University, (1965).

[62] Abramenko, V.L. and Sergienko, V.S., "Molecular complexes and chelates of dioxomolybdenum(VI) with salicylidene-4-iminobenzenesulfonamides: The crystal structures of salicylidene-4-iminobenzenesulfonamido-5-ethyl-1,3,4-thiadiazole (L-5) and its MoO2L25 complex", Russ. J. Inorg. Chem., 47(6):806-815, (2002).

[63] Balachandran, V. and Parimala, K., "Tautomeric purine forms of 2-amino-6-chloropurine (N9H10 and N7H10): Structures, vibrational assignments, NBO analysis, hyperpolarizability, HOMO-LUMO study using B3 based density functional calculations", Spectrochim. Acta A, 96: 340-351, (2012).

[64] Reed, A.E. and Weinstock, R.B., "Weinhold F Natural-Population Analysis", J. Chem. Phys., 83(2): 735-746, (1985).

[65] Politzer, P., Concha, M.C., Murray, J.S., "Density functional study of dimers of dimethylnitramine", Int. J. Quantum. Chem., 80(2): 184-192, (2000).

[66] Govindarajan, M., and Karabacak M., "Spectroscopic properties, NLO, HOMO-LUMO and NBO analysis of 2,5-Lutidine", Spectrochim. Acta A, 96: 421-435, (2012).

[67] Govindarajan, M., Periandy, S. and Carthigayen, K., "FT-IR and FT-Raman spectra, thermo dynamical behavior, HOMO and LUMO, UV, NLO properties, computed frequency estimation analysis and electronic structure calculations on alpha-bromotoluene", Spectrochim. Acta A, 97: 411-422, (2012).